ACS APPLIED MATERIALS & INTERFACES

Research Article

www.acsami.org

Performance of Dielectric Nanocomposites: Matrix-Free, Hairy Nanoparticle Assemblies and Amorphous Polymer–Nanoparticle Blends

Christopher A. Grabowski,[†,‡] Hilmar Koerner,[†] Jeffrey S. Meth,[§] Alei Dang,[▽] Chin Ming Hui,[▽] Krzysztof Matyjaszewski,[▽] Michael R. Bockstaller,[⊥] Michael F. Durstock,[†] and Richard A. Vaia*[,†]

[†]Materials and Manufacturing Directorate, Air Force Research Laboratory, Wright-Patterson Air Force Base, Ohio 45433, United States

[‡]UES, Inc., Dayton, Ohio 45432, United States

[§]DuPont Central Research & Development, E.I. DuPont de Nemours & Co., Inc., Wilmington, Delaware 19880, United States

[▽]Department of Chemistry, Carnegie Mellon University, Pittsburgh, Pennsylvania 15213, United States

[⊥]Department of Materials Science and Engineering, Carnegie Mellon University, Pittsburgh, Pennsylvania 15213, United States

Supporting Information

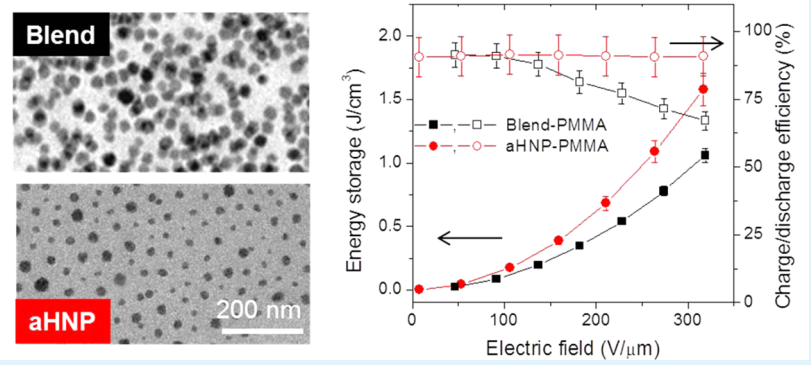

ABSTRACT: Demands to increase the stored energy density of electrostatic capacitors have spurred the development of materials with enhanced dielectric breakdown, improved permittivity, and reduced dielectric loss. Polymer nanocomposites (PNCs), consisting of a blend of amorphous polymer and dielectric nanofillers, have been studied intensely to satisfy these goals; however, nanoparticle aggregates, field localization due to dielectric mismatch between particle and matrix, and the poorly understood role of interface compatibilization have challenged progress. To expand the understanding of the inter-relation between these factors and, thus, enable rational optimization of low and high contrast PNC dielectrics, we compare the dielectric performance of matrix-free hairy nanoparticle assemblies (aHNPs) to blended PNCs in the regime of low dielectric contrast to establish how morphology and interface impact energy storage and breakdown across different polymer matrices (polystyrene, PS, and poly(methyl methacrylate), PMMA) and nanoparticle loadings (0–50% (v/v) silica). The findings indicate that the route (aHNP versus blending) to well-dispersed morphology has, at most, a minor impact on breakdown strength trends with nanoparticle volume fraction; the only exception being at intermediate loadings of silica in PMMA (15% (v/v)). Conversely, aHNPs show substantial improvements in reducing dielectric loss and maintaining charge/discharge efficiency. For example, low-frequency dielectric loss (1 Hz–1 kHz) of PS and PMMA aHNP films was essentially unchanged up to a silica content of 50% (v/v), whereas traditional blends showed a monotonically increasing loss with silica loading. Similar benefits are seen via high-field polarization loop measurements where energy storage for ∼15% (v/v) silica loaded PMMA and PS aHNPs were 50% and 200% greater than respective comparable PNC blends. Overall, these findings on low dielectric contrast PNCs clearly point to the performance benefits of functionalizing the nanoparticle surface with high-molecular-weight polymers for polymer nanostructured dielectrics.

KEYWORDS: *polymer-grafted nanoparticles, colloidal silica, dielectric breakdown, permittivity, energy storage, capacitor*

INTRODUCTION

Energy storage solutions are not keeping pace with the demand for high-performance, ultrasmall, portable electronics.[1] Electrostatic capacitors are of particular importance for applications

Received: September 22, 2014
Accepted: November 3, 2014
Published: November 3, 2014

requiring rapid switching of high energy density; however, current components cannot deliver sufficient energy in a compact form factor for many medical, transportation, and aerospace applications.[2] Most commercial capacitors employ low permittivity (ε_r = 2−5), high breakdown (E_{BD} > 600 V/μm) plastic dielectrics, such as biaxially oriented polypropylene (BOPP) or polyester. These materials have a maximum theoretical energy density ($u = 1/2\varepsilon_o\varepsilon_r|E_{BD}|^2$) of ∼4 J/cm^3. Subsequent packaged capacitors have energy densities of <2 J/cm^3, at least 2−5 times less than emerging requirements. To improve performance, the energy density of the dielectric must be enhanced in a manner that increases permittivity, provides predictable and graceful failure at higher fields, and maintains the ability to manufacture large-area, defect-free films.

Polymer nanocomposites (PNCs) have been extensively examined toward these ends.[3−20] Conceptually, the dispersion of a high-permittivity inorganic nanoparticle (NP) into a polymer with large dielectric breakdown strength affords the combination of the processability and flexibility of a polymer while maintaining a nanoscopic morphology that may simultaneously enhance dielectric breakdown strength and dielectric permittivity. However, in practice, this rarely occurs. Although blending high-permittivity ceramic fillers (such as $BaTiO_3$ and TiO_2) with a polymer increases the permittivity consistent with effective medium theories such as the Bruggeman model, concomitant reductions in breakdown strength and dielectric loss offset any potential gains in the theoretical energy storage density.[7,21−23] Such trends are consistent with finite difference simulations, which predict a 50% reduction in breakdown strength for 40% (v/v) $BaTiO_3$ PNCs.[7,8] The large dielectric mismatch between nanoparticle and surrounding matrix results in field intensification in the polymer matrix near the particle surface. This either enhances the local probability of dielectric failure or propagation of the discharge cascade.

Numerous concepts to circumvent this conundrum—while maintaining large-scale film processability—have been met with a variety of successes, including surface-modified nanoparticles,[9,13,17,18] aligned anisotropic fillers,[10,14−16,19] ferroelectric fillers,[11] and core−shell nanoparticles.[12] For example, while micrometer-sized silica inclusions drastically reduce the bulk polymer breakdown strength, a 5% (w/w) addition of silica nanoparticles was demonstrated to improve dielectric strength by ∼20% (increasing from 269 V/μm to 314 V/μm).[13] The improved performance, which is attributed to the reduced scale of the morphology, is consistent with BOPP, where increasing structural feature sizes (spherulite size, lamellar thickness, etc.) tends to reduce breakdown strength.[24] Similarly, interwoven nanoarchitectures arising from the dispersion and alignment of layered, low dielectric fillers such as montmorillonite[14−16] or boron nitride[19] have been shown to increase the breakdown strength relative to the unfilled polymer by 30%−80%. Tailoring the polymer/matrix interface has also shown benefits to dielectric performance. For example, a 2-fold increase in breakdown strength was recently reported when comparing poly(methyl methacrylate) (PMMA)-grafted $BaTiO_3$ composite films to a traditional PMMA/$BaTiO_3$ blend.[17,18] Fundamentally, these approaches attempt to diffuse field enhancement by modifying the composition, morphology, or interface, with respect to carrier generation or transport. However, the underlying mechanism(s) are unclear.[20] For example, what characteristics of the composition and morphology enhance or retard propagation or act as trap centers or carrier generators? How do these events depend on nanoparticle order, permittivity contrast, or nanoparticle−polymer interfacial interactions? Understanding these factors will be the key to guiding formulation of PNC dielectrics and establishing practical limits to performance enhancement.

Considering just one of these challenges, if polymer−nanoparticle interactions impact dielectric failure, then the performance should not only depend on the composition and dispersion of the inorganic, but also on the composition of the matrix in which the NP is dispersed. Recently, this effect was observed for four high-purity amorphous polymer films (PMMA, polystyrene (PS), polyimide (PI), and poly-4-vinylpyridine (P4VP)) uniformly incorporating the same dispersed silica colloid (up to 45% (v/v)).[20,25] Silica dispersion in polymers with a breakdown strength higher than that of silica (i.e., PMMA and PI) resulted in a reduction in performance, compared to the unfilled polymer, whereas the opposite effect (retention or increase in performance) was seen for silica addition to polymers with lower breakdown strength (P4VP and PS). For ∼15% (v/v) or greater silica content, all the PNC films exhibit breakdown at similar electric fields, implying that, at the highest loadings, failure becomes independent of polymer matrix. However, further understanding these observations and their extrapolation to systems with high particle/matrix permittivity contrast necessitates greater control of the nanoparticle morphology and the composition of the particle/matrix interface than utilized in these prior studies. For example, although the silica particles were qualitatively well-dispersed, especially in relation to the majority of PNC reports, the formation of inhomogeneities was still observed. In addition, the polymer/silica interface was dominated by van der Waals interactions, rather than specific chemical coupling or functionalization.

To clarify the importance of local nanoparticle order and the coupling between the nanoparticle and matrix, we compare herein the dielectric strength, complex dielectric permittivity, and energy storage efficiency of low dielectric contrast traditional PNC blends and bulk assemblies of matrix-free hairy (i.e., polymer-grafted) silica nanoparticles (aHNPs).[26,27] The polymer-grafted nanoparticle assemblies ensure a narrow distribution of particle−particle spacing, with a minimum interparticle spacing equal to or greater than the thickness of the grafted polymer canopy. In addition, polymers with relatively low (PS) and high (PMMA) breakdown strength are examined. The low particle/matrix permittivity contrast of silica filler minimizes amplification effects due to local field enhancement. Surprisingly, the traditional blends and aHNPs exhibited similar trends in breakdown strength with the exception of intermediate loading of silica in PMMA (15% (v/v)). This implies that there is a point of diminishing returns for continual morphology refinement in low-dielectric contrast nanocomposites. Significantly, however, the grafted architectures of HNPs positively impacted the complex dielectric permittivity. The covalent polymer grafts reduced dielectric loss and led to narrower $D-E$ hysteresis loops, demonstrating that interface modification is a key factor to greater capacitive performance at higher applied fields.

EXPERIMENTAL METHODS

Silica Nanocomposite Film Preparation. Detailed synthesis for polymer-grafted hairy silica nanoparticles (aHNPs) is available in ref 28. In brief, silica colloids obtained from Nissan Chemical Corp. (30% w/w silica in methyl isobutyl ketone, MIBK-ST) with a diameter of d

≈ 16 nm and a polydispersity index of 0.3 were used as received. A "grafting-from" approach was employed, wherein the ATRP initiator 1-(chlorodimethylsilyl)propyl-2-bromoisobutyrate was tethered to the silica NP surface. The polymer chains were then grown from these initiation sites through a surface-initiated atom transfer radical polymerization (SI-ATRP).[29−31] Table 1 summarizes the hairy nanoparticles investigated in this study. To reach a silica volume fraction range between 0.7% and 50%, we prepared particles with graft densities ranging from 0.07 chains/nm^2 to 0.61 chains/nm^2 and a molecular mass between 10 kg/mol and 840 kg/mol. Thin PNC films were prepared by flowcoating a ∼10% w/w solution of grafted particles dispersed in toluene onto an indium-doped tin oxide (ITO) glass substrate and subsequently annealed under vacuum at 120 °C for 24 h. This produced films 3−4 μm thick, as measured via profilometry (Bruker).

Table 1. Characteristics for Traditional Blended and Matrix-Free Hairy (Polymer-Grafted) Nanoparticle PNCs

sample	SiO_2 fraction (v/v)	degree of polymerization	graft density (chains/nm^2)
blend-PS-1	1.0	5500	
blend-PS-7.5	7.5	5500	
blend-PS-15	15.0	5500	
aHNP-PS-1	0.97	2200	0.57
aHNP-PS-4	4.35	520	0.57
aHNP-PS-18	18.1	100	0.61
aHNP-PS-50	50.0	192	0.07
blend-PMMA-1	1.0	3100	
blend-PMMA-7.5	7.5	3100	
blend-PMMA-15	15.0	3100	
blend-PMMA-30	30.0	3100	
blend-PMMA-45	45.0	3100	
aHNP-PMMA-1	0.7	6000	0.30
aHNP-PMMA-8	7.9	650	0.27
aHNP-PMMA-16	16.3	390	0.20
aHNP-PMMA-48	48.0	200	0.08

The synthetic procedure for traditional polymer/silica blend films is presented in ref 25. Ludox AS-40 (Aldrich) colloidal silica (d = 29 nm and polydispersity index = 0.11), which is solvent transferred into dimethylformamide (DMF), was used for blend samples. While different sources were used to prepare the blend and aHNP composites, NMR studies verify that the particles have the same bulk chemical composition. Dispersion of colloidal silica into PS was facilitated with a phenyltrimethoxysilane (Aldrich) capping agent on the nanoparticle (NP) surface, while the silica used for PMMA blends was left untreated with its native hydroxyl surface functionality. Polar nonaqueous solvents, such as DMF, helps forestall aggregation during composite formation by creating a charge-stabilized environment for the silica. The polymer/colloid/solvent mixture was coated onto 7 in. × 7 in. aluminum-coated glass—heated to 100 °C—using a 6-mil doctor blade. This heating process helps to further suppress aggregation due to sample kinetic factors. This procedure yielded films 5−6 μm thick, as measured via profilometry.

Samples for transmission electron microscopy (TEM) studies were prepared as follows. For traditional blends, the PNC mixture was first flowcoated onto a Kapton substrate and dried with the same procedure used for the samples on aluminum-coated glass. A layer of unfilled PMMA or PS (depending on the sample) was laminated to the sample as an encapsulant to protect the sample from the potting compounds used in TEM preparation. The laminate was then potted and microtomed to produce a sample with a cross-sectional thickness of ∼90 nm. For aHNP samples, a 1 mg/mL aHNP/toluene solution was dropcast onto a carbon-coated copper grid and annealed under vacuum at 120 °C for 24 h to form approximately monolayer films. An electron microscope (JEOL, Model EX2000) operated at 200 kV was used to image the films. Imaging was performed by using amplitude and phase contrast, and images were acquired using a high-resolution camera (Gatan, Model Orius SC600).

Small-angle X-ray scattering (SAXS) experiments were carried out on a three-pinhole SAXS system (Rigaku, Model S-MAX 3000) set to transmission mode at a sample/detector distance of 150 cm. Two-dimensional (2D) images were reduced using Nika 1 macros for Igor Pro.[32] Images were corrected for transmission, background, and initial beam intensity fluctuations. The SAXS data were further analyzed using the Irena analysis package.[33] The form factor for a sphere with log-normal distribution was used to fit the solution data of the aHNPs (parameters are relative volume fraction, breadth of the size distribution, and sphere radius). The SAXS data for aHNP films was analyzed and fitted using a combination of sphere form factor (obtained from solutions) and a Percus and Yevick[34] hard-sphere model.

Dielectric and Electrical Characterization and Modeling. Details of the dielectric breakdown, permittivity, and energy storage measurements are discussed below. Dielectric breakdown trials were performed using a 10 kV high-voltage supply (Spellman, Model SL300) controlled by a ramping circuit. The ramp was set such that a breakdown event occurs at ∼20 s, in accordance to ASTM standard protocol for short-term dielectric strength tests (which corresponds to 50−300 V/s, depending on the sample).[35] Once a current of >1 mA passes through the device, a silicon rectifier switch activates and breaks the circuit. The breakdown voltages were read from a multimeter (Fluke, Model 289) set in peak capture mode.

Our experimental geometry features a copper rod with a hemispherical end (radius of curvature = 2.5 mm) that makes direct contact with the PNC film. Breakdown is confined to a small sample region (area of ∼0.1 cm^2) in an attempt to remove the influence of film heterogeneity by spatially localizing the electric field. At least 15 breakdown trials were performed for each film to conduct Weibull failure analysis. The copper contact rod was polished after every 15 breakdowns using diamond paste to remove pitting.

Free-standing BOPP film was periodically employed as a test standard to ensure our experimental platform remained calibrated. A value of 800 V/μm was obtained for characteristic dielectric strength, which is comparable to results previously reported in the literature.[36] All experiments were conducted at room temperature in an N_2 purged environment where relative humidity was observed in the range of 10%−20%. Breakdown voltages were converted to breakdown strength by measuring film thickness near each test site via profilometry.

Dielectric impedance and permittivity measurements were conducted on all PNC films using a Novocontrol Alpha Analyzer. A circular aluminum contact 1 cm in diameter and 200 nm thick was deposited onto each film, whereupon a drop of colloidal silver was placed to prevent damage to the aluminum film. Thin needle probes rested on the colloidal silver contact points to facilitate the measurements, which were conducted in an N_2 purged environment at room temperature. Permittivity was measured at discrete frequencies, swept over the range from 1 Hz to 1 MHz at an AC driving voltage of 1 V.

Energy storage measurements were conducted on PNC films using a Premier II ferroelectric tester (Radiant Technologies, Inc.). Electrodes utilized for these tests are equivalent to those employed for permittivity tests. Voltage was linearly ramped from zero to maximum and back to zero in 10 s while the corresponding electric displacement response is measured. The resulting displacement field-electric field (D−E) hysteresis loops are integrated to determine energy density and charge/discharge efficiency.

Modeling of PNC electric field distributions was performed using the commercial software packages COMSOL Multiphysics and Mathematica. Nanoparticles were represented as 2D circles of fixed diameter and permittivity, distributed in a uniform dielectric slab. Parallel conductive plates used to apply the external DC field are placed suitably far away to prevent fringing effects and field concentration near sharp corners. A Mathematica routine employing a random number generator distributes particles with a minimum distance between neighboring particles set by the user. The electric

field distributions were plotted as 2D heat maps, where color denotes the magnitude of the local field relative to the applied field.

RESULTS AND DISCUSSION

Figure 1 compares the preparation, structure, and morphology of traditional polymer–silica nanocomposites with assemblies

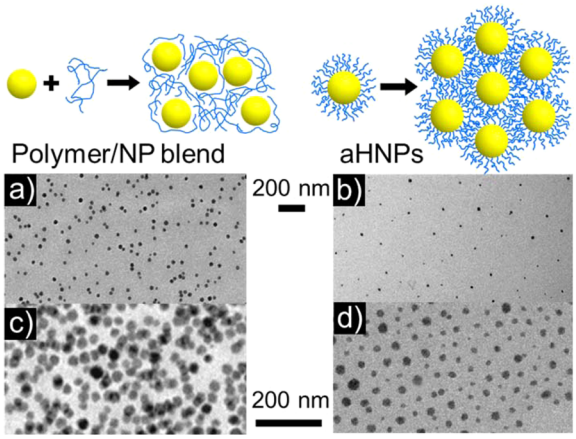

Figure 1. (Top) Illustrations of a polymer/nanoparticle blend (traditional PNCs) and assembled hairy nanoparticles (aHNPs). (Bottom) Representative transmission electron microscopy (TEM) images of PMMA/silica films: (a) blend 1% (v/v) loading, (b) aHNP 0.7% (v/v), (c) blend 15% (v/v), and (d) aHNP 16% (v/v). Note that, because of the fabrication approach for the blends, ~90 nm microtome slices were prepared for TEM analysis. Images therefore reflect the projection of silica distribution both in-plane and through the slice thickness (~3.5 nanoparticle (NP) diameters). Thus, differentiating between actual clusters of a few NPs and image projection artifacts is challenging, and becomes moreso as the volume fraction increases. In contrast, the single component nature of the aHNPs enables solution casting to fabricate both monolayer slices (20 nm) for TEM, as well as micrometer-thick films for dielectric evaluation.

of matrix-free hairy silica nanoparticles (aHNPs). Nanocomposites of both types were prepared with polystyrene (PS) and poly(methyl methacrylate) (PMMA) anchored chains. PS is a nonpolar polymer with relatively poor breakdown strength (400 V/μm) and low dielectric loss ($\varepsilon'' \approx 10^{-3}$ at 1 kHz), while PMMA is a highly polar polymer with excellent breakdown strength (800 V/μm) and high dielectric loss ($\varepsilon'' \approx 10^{-1}$ at 1 kHz). The real permittivities of PS ($\varepsilon' \approx 2.6$) and PMMA ($\varepsilon' \approx 3.0$) are similar, and comparable to silica ($\varepsilon' \approx 3.9$). The traditional nanocomposite blends have well-dispersed, randomly distributed silica with a small fraction of few-particle aggregates (Figure 1), which is consistent with prior reports on this solvent-based fabrication procedure.[25] In contrast, aHNPs generally exhibit a more-ordered morphology with no particle aggregates due to the covalent grafting of polymers from the silica surface.[37−39] The inorganic volume fraction within aHNPs can be varied without resorting to adding free polymer by adjusting the polymer molecular weight and graft density.[38−40]

More quantitative comparisons of the morphology are provided by small-angle X-ray scattering (SAXS) from 3 μm films used for dielectric testing (Figure 2). Although the aHNPs exhibit better order than their blend counterparts at low loading (<15% (v/v) silica), they fail to order as extensively as colloidal crystals[41] or ligand-functionalized nanoparticle supracrystals.[42] This is evidenced by the value of the structure factor at the initial peak for the aHNP films falling well short of the values of crystalline materials (such as colloidal crystals), instead reaching 0.2−0.3. This is most likely due to the relatively large size disparity of the core silica particle (d = 16 +3/−5 nm). No agglomeration is detected from the X-ray scattering at low q. $S(q \approx 0)$ also decreases systematically with silica loading, which is expected for simply packed particles that are homogeneously dispersed. Particle–particle distance in the aHNPs, as reflected in the location of the initial peak of the structure factor $S(q)$, increases as the silica content increases, and is at least 5 nm in all samples. In contrast, the traditional PNC blends have a lower value of the initial correlation peak of the structure factor (<0.1) and show signs of particle clustering, as seen by oscillations at higher q values that shift marginally with silica loading and are comparable to nanoparticle diameter. However, compared to many PNCs, the general dispersion of these blends is good, and large-scale aggregation is avoided, as indicated by the finite value of $S(q \approx 0)$ and the almost-nonexistent intensity increase at low q (USAXS data are presented in Figure S1 in the Supporting Information). To summarize, both PNC blends and aHNPs exhibit excellent silica dispersion; however, the "uniformity", as measured by the narrowness of the distribution of interparticle separation, is slightly better for the aHNPs.

The real dielectric permittivity (ε'), measured at 100 kHz, is shown in Figure 3 (full frequency sweeps are presented in Figure S2 in the Supporting Information). Neat polymer films displayed permittivities close to the literature values. The real dielectric permittivity (ε') increases monotonically with higher silica loadings, approximately following the Bruggeman Effective Medium Approximation (EMA),[43] assuming a silica permittivity of 3.9. However, PMMA blends systematically exhibit slightly higher permittivities. Such a trend is consistent with previously investigated blends of $BaTiO_3$ NPs in PMMA.[9] The loss tangent (tan δ), measured at 1 Hz and 1 kHz, is compared in Figure 4 (full frequency sweeps are presented in Figure S2 in the Supporting Information). Traditional PNC blends exhibit increasing dielectric loss for higher silica loading, especially at low frequency. Alternatively, aHNPs show no change in loss,even at 50% (v/v) silica loading, irrespective of the grafted polymer. As a comparison, blends incorporating 15% (v/v) silica into PS, which is a nonpolar, low-dielectric-loss polymer, increase the dielectric loss by nearly an order of magnitude at frequencies below 1 kHz; whereas PS aHNPs show practically no influence of silica loading on loss. Similarly, PMMA, which is a highly polar polymer with relatively high dielectric loss, follows similar trends, albeit the difference between blends and aHNPs at higher frequencies is not as pronounced.

Morphology is a possible explanation of these dielectric results. The onset of percolative networks in random sphere packing occurs at ~15%–20% (v/v).[7,44] At this point, fractal and long-range correlations, which are absent in the Bruggeman formalism, become important and result in a proportionately greater increase in effective permittivity. These spanning clusters would also lead to extended paths for interface charge migration and, thus, low-frequency loss. This behavior has been previously observed in blends of silica microparticles and nanoparticles in cross-linked polyethylene.[45] The presence of grafted polymer guarantees a finite particle–particle separation, inhibiting these processes. However, no evidence of extensive aggregation is seen in either PMMA or PS; therefore, morphology is an unlikely cause. Alternatively, local charge

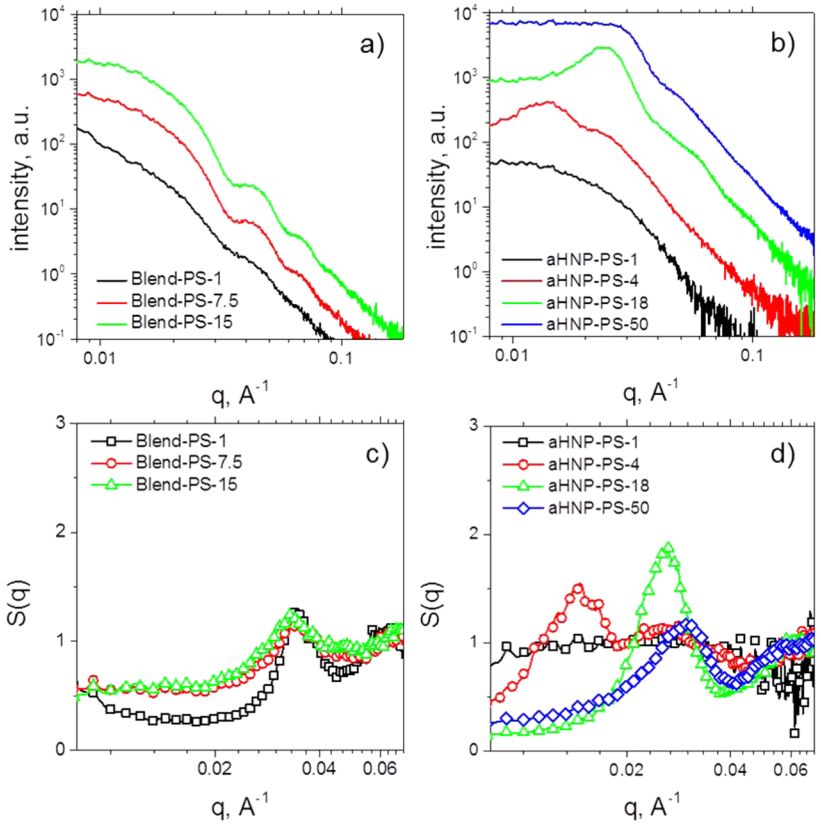

Figure 2. (a, b) Representative small-angle X-ray scattering (SAXS) intensity and (c, d) corresponding structure factor, $S(q)$, for blend-PS-X (X = 1, 7.5, 15) (panels (a) and (c)) and aHNP-PS-X (X = 1, 4, 18 and 50) (panel (b) and (d)). Structure factor is obtained from scattering curves by normalizing with form factor of isolated nanoparticle. Sample ID and associated details are found in Table 1.

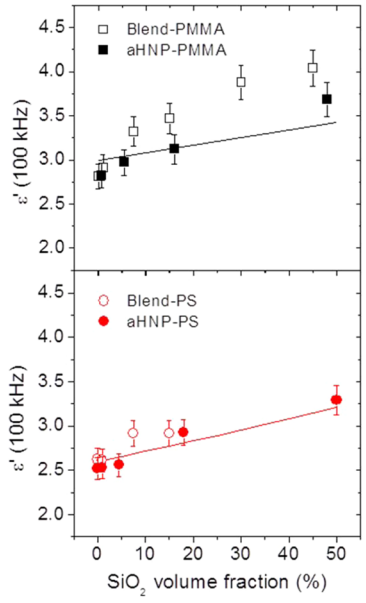

Figure 3. Real dielectric permittivity at 100 kHz for PMMA (black squares) and PS (red circles) PNCs. Blends are represented by open shapes and aHNPs are represented by filled shapes. Error bars represent uncertainty in film thickness and impedance measurement reproducibility. Lines correspond to the Bruggeman Effective Medium Approximation (EMA), using literature values for silica nanoparticles ($\varepsilon' = 3.9$), PMMA ($\varepsilon' = 3.0$), and PS ($\varepsilon' = 2.6$).

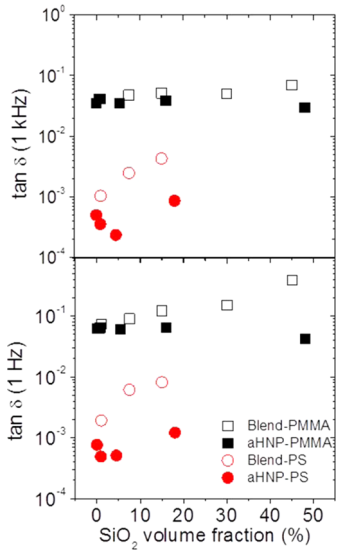

Figure 4. Dielectric loss (tan δ) for PS (denoted by red circles) and PMMA (denoted by black squares) PNCs with varying silica loading at frequencies of 1 kHz (top plot) and 1 Hz (bottom plot). Blends are represented by open shapes, and aHNPs are represented by filled shapes.

separation at internal dielectric interfaces could manifest in a silica dependent low-frequency relaxation at room temperature.[4] This interfacial (e.g., Maxwell–Wagner) relaxation would increase permittivity above EMA estimates, since this emergent polarization is not taken into account in the Bruggeman formalism. Similarly, very low-frequency ionic conductivity could also increase effective dielectric response.

The high-frequency tail of a very low-frequency relaxation, which increases with silica-volume fraction, is evident in the impedance spectra of the PMMA-silica blends from 0.1 to 100 Hz (Figure S2 in the Supporting Information), but absent in the comparable aHNP spectra. At this point, the molecular process underlying this additional relaxation is unclear, but most likely is associated with the different composition and structure of the silica interface in the PMMA blend (native hydroxyl surface) and aHNP (silane-modified). Others have also noted that coating dispersed particles with an insulating layer reduces dielectric loss in traditional nanocomposites.[46,47] Overall, the different dielectric response of blends and aHNPs, irrespective of the polymer, highlights the importance of chains grafted to the nanoparticle, as well as providing an important indicator of the potential for improved dielectric energy storage performance with aHNPs.

Figures 5a and 5b compare the characteristic dielectric breakdown strength (E_{BD}) observed for the blend and aHNP films. The experimental failure data (see Figures S3 and S4 in the Supporting Information) was modeled using a two-parameter Weibull cumulative probability function:

$$P(E) = 1 - \exp\left[-\left(\frac{E}{E_{BD}}\right)^{\beta}\right]$$

where $P(E)$ is the cumulative probability for failure, E is the experimental breakdown strength, E_{BD} reflects the electric field where there is 63.2% probability for failure, and β is the shape parameter associated with the least-squares fit of the distribution. Error bars in Figures 5a and 5b represent one standard deviation of the acquired breakdown data.

Overall, the breakdown strength of both PS and PMMA blends and aHNP films have similar trends with increasing silica fraction. E_{BD} ranges from 390 V/μm for a neat PS film up to a maximum of 470 V/μm for the 4.5% (v/v) aHNP sample (molecular weight of Mw = 60 000, graft density of 0.57 chains/nm^2) and 460 V/μm for the 7.5% (v/v) traditional blend. Both PS PNCs have a characteristic breakdown strength of ~400 V/μm near 15% (v/v), which then drops to 300 V/μm at 50% (v/v). The consistency between these very different systems is important to note and indicates that the slightly more-ordered morphology in the case of aHNP samples does not significantly impact the dielectric failure mechanisms. In stark contrast to the PS nanocomposites, PMMA HNPs show a significant decline in breakdown strength at very low volume fraction: from 800 V/μm for neat samples, down to 630 V/μm for 0.7% (v/v) samples (Mw = 840 000, graft density = 0.30 chains/nm^2), which also mirrors the behavior of PMMA blends. Breakdown strength shows a decline toward a value of 350 V/μm at 48% (v/v) loading (Mw = 24 000, graft density = 0.08 chains/nm^2), which is equivalent to the decline seen for the 45% (v/v) loaded PMMA blend. The only exception to these general similarities is observed at an intermediate loading of ~15% (v/v), where the PMMA aHNP (Mw = 47 000, graft density = 0.20 chains/nm^2) has an E_{BD} value of 520 V/μm, which is a 47% improvement over the comparable PMMA blend. These results indicate that adopting aHNP architectures does not translate to improved breakdown performance at high inorganic loading fractions. The dielectric strengths of all aHNPs and blends studied reach values of 300–350 V/μm at sufficiently high loadings (>45% (v/v)), indicating that failure has become matrix-independent and the filler dominates the breakdown behavior.

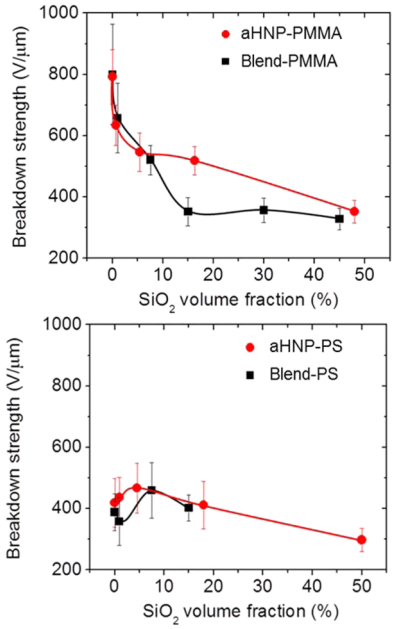

Figure 5. Characteristic breakdown strength (E_{BD}) as a function of silica volume fraction for PMMA and PS PNC films (top and bottom, respectively). Blends are represented by black squares and aHNPs are represented by red circles. E_{BD} values correspond to a 63.2% failure probability from Weibull analysis. Error bars represent one standard deviation of the E_{BD} values measured across >15 breakdown tests.

Energy storage density and charge/discharge efficiency, obtained by integrating $D-E$ polarization loops, are plotted for intermediate silica loading (~15% (v/v)) in Figure 6, as a function of applied electric field (see Figure S5 in the Supporting Information for full hysteresis loops). The aHNP and blend PMMA samples show comparable efficiency and energy storage behavior at low applied fields (<100 V/μm). When moving to higher fields, the aHNP film maintains a consistent 90% charge/discharge efficiency, but the blend sample experiences a reduction in efficiency down to 67% at an applied field of 320 V/μm. This is reflected in the maximum energy storage obtained for these films; the PMMA blend film stores 1.06 J/cm^3 at 320 V/μm, while the aHNP PMMA film can store 1.58 J/cm^3 at the same applied field—an improvement of almost 50% over the blend sample performance. Similar trends are observed for the PS PNC films. At an applied field of 204 V/μm, the aHNP sample delivers 0.57 J/cm^3, which is more than twice the maximum storage of a PS blend with comparable silica loading (0.23 J/cm^3). Again, this large difference is caused by charge/discharge inefficiencies experienced by the blend sample (46% vs 99% for PS-aHNP at 204 V/μm) when applying a large electric field to the film. Coupled with the dielectric loss data reported earlier for these systems (in which films are subjected to an AC potential of 1 V), we can conclude that increasing the silica loading negatively impacts the loss and storage efficiency of blend architectures, whereas aHNP films show no influence up to 50% (v/v) loading.

Two complementary factors must be considered to understand these results: the impact of nanoparticle dispersion and the role of the nanoparticle/polymer interface. Dielectric breakdown is a defect-driven event where initiation occurs when a high local field from particle clustering or electrode roughness is commensurate with a region of weaker dielectric

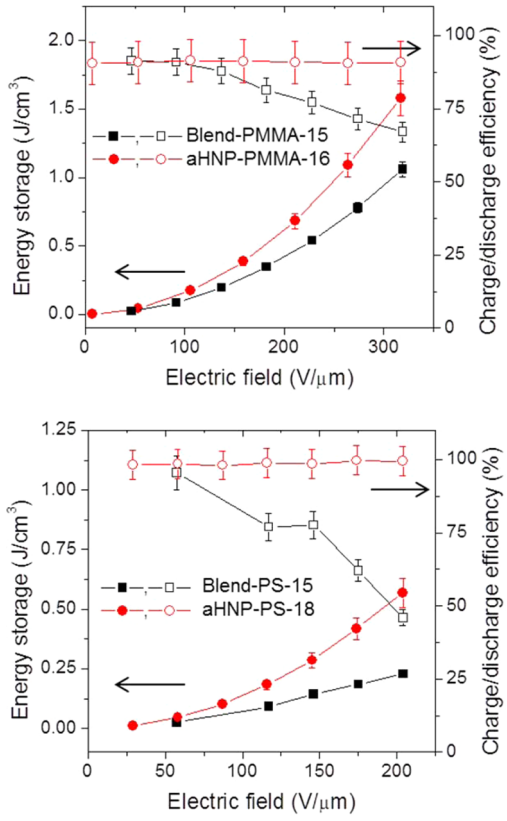

Figure 6. (Top) Energy density and charge/discharge efficiency determined from $D-E$ polarization loops for aHNP-PMMA-16 and blend-PMMA-15 films, plotted against applied electric field. (Bottom) Energy density and charge/discharge efficiency for aHNP-PS-18 and blend-PS-15 films.

strength, such as small molecule impurity, low matrix density, void or even the particle inclusion itself.[4,48] In a previous publication, we noted how silica impacts breakdown differently, depending on the polymer matrix polymer, because of the dielectric strength and work function of the silica relative to the polymer.[20] Silica in PS tends to inhibit propagation of the failure cascade, because of the relative higher polarity of the silica inclusions. This ultimately improves the dielectric strength over its bulk counterpart. Alternatively, PMMA has a higher inherent polarity, compared to the dispersed silica. In this case, silica acts as a defect, reducing the dielectric strength.

Revisiting the dielectric failure tests, both blends and hairy composites showed similar breakdown behavior. So, we can infer that (i) the characteristics of the particle and silica dominate and (ii) the increased dispersion and local structural ordering afforded by aHNPs over the solvent-dispersed PNCs is inconsequential. The clusters present in the blends appear to be small enough not to impact dielectric initiation/propagation. Effectively, improving order and dispersion above a threshold results in diminishing returns to dielectric strength. The initiation of breakdown events is aided greatly by the presence of highly localized fields, which are generated by the dielectric mismatch of nanofiller and the surrounding matrix.[8,49] The field exclusion behavior of PNCs is visualized in Figure 7, which shows the simulated electric field distribution for two cases of randomly distributed particles with and without grafted chains. In the latter case, the grafts ensure a particle separation of greater than one radius. First, consider a high dielectric contrast hybrid with $\varepsilon_{NP}/\varepsilon_{poly}$ = 100 (Figure 7a, representative of PMMA/$BaTiO_3$). Field-induced dipoles within the particles lead to the overlapping of excluded fields between particles in close proximity. Local fields may reach strengths many times greater than the magnitude of the initially applied field in the direction of the applied field, resulting in "extended clusters" with "hot spots." These extended regions of high field are the most likely to fail and initiate dielectric breakdown. Increasing particle-particle separation with a polymer graft (Figure 7b) reduces the size of these "extended clusters", lowering both the maximum field enhancement (i.e., no "white" regions with E/E_0 > 3) and the volume fraction of regions with significant field intensification. This intuitive understanding of particle morphology is consistent with dielectric studies of PMMA/$BaTiO_3$ aHNP films, where breakdown was improved 2-fold over traditional PMMA/$BaTiO_3$ blends.[17] On the other hand, for low dielectric contrast hybrid with $\varepsilon_{NP}/\varepsilon_{poly}$ = 1.5 (representative of PMMA/silica) the simulations do not show any appreciable difference in field distribution between randomly distributed particles without an interface buffer (Figure 7c) and with an interface buffer (Figure 7d). Thus, the enforcement of a minimum particle−particle separation does not translate into a more homogeneous internal field, since, effectively, there is minimal field exclusion from the low-dielectric constant filler. This is consistent with the results discussed herein, as well as previous studies.[20] Whether uncapped, phenyltrimethoxysilane-surface-modified or polymer-rafted silica, breakdown trends are more dependent on polymer composition, rather than interface functionalization. As previously proposed, it does not appear that grafting polymer chains to nanoparticle surfaces provides a respite in mitigating dielectric breakdown.

In contrast to the breakdown behavior, the dielectric loss and discharge efficiency of aHNPs and blends are drastically different. In traditional blends, the native hydroxyl surface functionality (in PMMA) or a small molecular weight capping agent (in PS) does not suppress interfacial dielectric relaxation processes. Grafted macromolecules, in addition to preventing agglomeration, lead to lower conduction between particles and may also reduce charge movement throughout the film. Surface functionalization and other particle coatings have been actively discussed in the literature as a means of improving dielectric performance.[12,23,50] Generally, this improved performance may reflect a more-complete capping of surface chemical species on the colloidal silica by the polymer grafting procedure, or the formation of a robust insulative barrier around the particle surface due to the polymer. However, the coherency of results across different silica, surface functionalization approaches, and matrices support the latter hypothesis. Overall, our results confirm that macromolecular interface modification significantly mitigates dielectric loss and improves energy storage efficiency.

CONCLUSIONS

The dielectric response, breakdown characteristics, and energy storage efficiency of low-dielectric constant polymer nanocomposite (PNC) blends and matrix-free hairy nanoparticle assemblies (aHNPs) exhibit both similarities and differences. Understanding the source of both is key to balancing the morphology, composition, and interface factors in the design of future dielectrics for high power capacitors. From a morphology standpoint, films of aHNP and blends both achieve excellent silica dispersion. Furthermore, minor differences in local order and particle separation do not manifest in

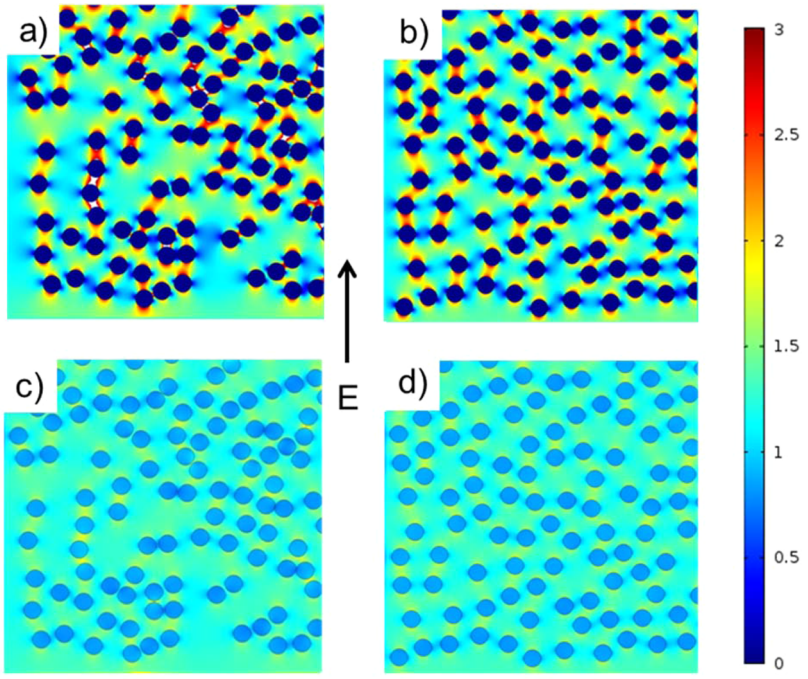

Figure 7. Two-dimensional (2D) simulated electric field distributions for 100 particles with permittivity ratio of (a, b) 100:1 and (c, d) 1.5:1, with respect to the matrix. For each, two cases reflect randomly distributed particles with and without grafted chains. For chain grafting, the minimum particle separation is greater than one radius (panels (b) and (d)), whereas without grafting, the particle−particle separation may be less than one radius (panels (a) and (c)). Colors correspond to the normalized field intensity (E/E_0). White regions observed in panel (a) are areas where $E/E_0 > 3$.

substantially different internal electric field distribution when the dielectric contrast between particle and matrix is small. Thus, dielectric breakdown is similar. Any improvement in capacitive performance must be attributed to more than hairy nanoparticles limiting larger-scale agglomeration. Energy storage and its efficiency also are dependent on dielectric loss processes. Here, polymer grafting and aHNPs are distinct from traditional blends. The low-frequency dielectric loss of polystyrene (PS) and poly(methyl methacrylate) (PMMA) aHNP films show no change for increasing silica content up to 50% (v/v), which contrasts with the PS and PMMA silica blends that generate significantly higher losses for increased silica loading. PS and PMMA aHNP samples at intermediate (15% (v/v)) silica loadings were found to maintain high charge/discharge efficiency (90+%) at high applied fields, while PS and PMMA blends begin to show an efficiency dropoff above 100 V/μm. Thus, aHNP films can ultimately deliver more energy than comparable blends, thanks to these improvements in loss behavior. However, the predominance of dielectric loss mitigation via interface structure over morphology may not hold as the dielectric constant between the matrix and the nanoparticle increases. Here, modeling showed that internal fields are much more sensitive to morphology. Thus, additional examples of high contrast aHNPs and PNC-blended system across various matrices, fillers, and interface modification techniques are required.

In summary, our direct comparison of PNC architectures illustrates a motivation in adopting a grafted polymer approach when producing films for dielectric applications. While traditional blend casting methods can yield well-dispersed particles with little aggregation, the losses generated at high inorganic fractions severely degrade energy delivery efficiency and, thus, maximum energy storage. The improvements in dielectric performance, coupled with the ease in casting large-scale films, demonstrate the usefulness of single-component hairy nanoparticle films in capacitor and energy storage technologies.

■ ASSOCIATED CONTENT

Ⓢ Supporting Information

USAXS data, complex dielectric permittivity scans for all aHNPs and blends, full aHNP breakdown data, and polarization loop comparisons between blends and aHNPs. This material is available free of charge via the Internet at http://pubs.acs.org.

■ AUTHOR INFORMATION

Corresponding Author

* E-mail: richard.vaia@us.af.mil.

Author Contributions

The manuscript was written through contributions of all authors.

Notes

The authors declare no competing financial interest.

■ ACKNOWLEDGMENTS

The authors wish to thank the Air Force Office of Scientific Research (AFOSR) and Air Force Research Laboratory Materials & Manufacturing Directorate for their financial support, along with V. McNeir and J. DeCerbo for their assistance with energy storage characterization, and Changzai Chi for colloidal silica samples. K.M. and M.R.B. acknowledge partial support from the National Science Foundation (NSF) (Nos. DMR 0969301 and CMMI-1234263) and AFOSR (No. FA9550-09-1-0169).

REFERENCES

(1) Whittingham, M. S. Materials Challenges Facing Electrical Energy Storage. *MRS Bull.* **2008**, *33*, 411−419.

(2) Cao, Y.; Irwin, P. C.; Younsi, K. The Future of Nanodielectrics in the Electrical Power Industry. *IEEE Trans. Dielectr. Electr. Insul.* **2004**, *11*, 797−807.

(3) Ducharme, S. An Inside-Out Approach to Storing Electrostatic Energy. *ACS Nano* **2009**, *3*, 2447−2450.

(4) Nelson, J. *Dielectric Polymer Nanocomposites*; Springer: New York, 2010.

(5) Dang, Z.-M.; Yuan, J.-K.; Yao, S.-H.; Liao, R.-J. Flexible Nanodielectric Materials with High Permittivity for Power Energy Storage. *Adv. Mater.* **2013**, *25*, 6334−6365.

(6) Wang, Q.; Zhu, L. J. Polymer Nanocomposites for Electrical Energy Storage. *J. Polym. Sci., Part B: Polym. Phys.* **2011**, *49*, 1421−1429.

(7) Kim, P.; Doss, N. M.; Tillotson, J. P.; Hotchkiss, P. J.; Pan, M.-J.; Marder, S. R.; Li, J.; Calame, J. P.; Perry, J. W. High Energy Density Nanocomposites Based on Surface-Modified $BaTiO_3$ and a Ferroelectric Polymer. *ACS Nano* **2009**, *3*, 2581−2592.

(8) Calame, J. P. Finite Difference Simulations of Permittivity and Electric Field Statistics in Ceramic−Polymer Composites for Capacitor Applications. *J. Appl. Phys.* **2006**, *99*, 084101.

(9) Xie, L.; Huang, Y.; Liu, F.; Huang, X.; Jiang, P., Comparative Investigation on Dielectric Property and Thermal Conductivity of In Situ Polymerized and Solution Mixed Polymer Nanocomposites. Presented at the *IEEE International Conference on Solid Dielectrics*, Bologna, Italy, 2013.

(10) Tang, H.; Malakooti, M. H.; Sodano, H. A. Relationship between Orientation Factor of Lead Zirconate Titanate Nanowires and Dielectric Permittivity of Nanocomposites. *Appl. Phys. Lett.* **2013**, *103*, 222901.

(11) Dang, Z.-M.; Yuan, J.-K.; Zha, J.-W.; Zhou, T.; Li, S.-T.; Hu, G.-H. Fundamentals, Processes and Applications of High-Permittivity Polymer−Matrix Composites. *Prog. Mater. Sci.* **2012**, *57*, 660−723.

(12) Fredin, L. A.; Li, Z.; Ratner, M. A.; Lanagan, M. T.; Marks, T. J. Enhanced Energy Storage and Suppressed Dielectric Loss in Oxide Core−Shell−Polyolefin Nanocomposites by Moderating Internal Surface Area and Increasing Shell Thickness. *Adv. Mater.* **2012**, *24*, 5946−5953.

(13) Roy, M.; Nelson, J. K.; MacCrone, R. K.; Schadler, L. S. Candidate Mechanisms Controlling the Electrical Characteristics of Silica/XLPE Nanodielectrics. *J. Mater. Sci.* **2007**, *42*, 3789−3799.

(14) Fillery, S. P.; Koerner, H.; Drummy, L.; Dunkerley, E.; Durstock, M. F.; Schmidt, D. F.; Vaia, R. A. Nanolaminates: Increasing Dielectric Breakdown Strength of Composites. *ACS Appl. Mater. Interfaces* **2012**, *4*, 1388−1396.

(15) Tomer, V.; Polizos, G.; Randall, C. A.; Manias, E. Polyethylene Nanocomposite Dielectrics: Implications of Nanofiller Orientation on High Field Properties and Energy Storage. *J. Appl. Phys.* **2011**, *109*, 074113.

(16) Brandstetter, S. S.; Drummy, L. F.; Horwath, J. C.; Schweickart, D. L.; Vaia, R. A. Breakdown Voltage of Thermoplastics with Clay Nanometer-Sized Fillers. In *Proceedings of the 2008 IEEE International Power Modulator High Voltage Conference*, Las Vegas, NV, 2008; pp 287−290.

(17) Paniagua, S. A.; Kim, Y.; Henry, K.; Kumar, R.; Perry, J. W.; Marder, S. R. Surface-Initiated Polymerization from Barium Titanate Nanoparticles for Hybrid Dielectric Capacitors. *ACS Appl. Mater. Interfaces* **2014**, *6*, 3477−3482.

(18) Fillery, S. P.; Kern, K.; Koerner, H.; Drummy, L.; Tchoul, M.; Beier, C.; Brutchey, R. L.; Durstock, M. F.; Vaia, R. A. Single Component $BaTiO_3$ Polymer Nanocomposites: Polymer−Nanoparticle Hybrids for Capacitive Energy Storage. Presented at the *ACS Spring Meeting*, San Diego, CA, 2012.

(19) Li, Q.; Han, K.; Gadinski, M. R.; Zhang, G.; Wang, Q. High Energy and Power Density Capacitors from Solution-Processed Ternary Ferroelectric Polymer Nanocomposites. *Adv. Mater.* **2014**, *26*, 6244−6249.

(20) Grabowski, C. A.; Fillery, S. P.; Westing, N. M.; Chi, C. Z.; Meth, J. S.; Durstock, M. F.; Vaia, R. A. Dielectric Breakdown in Silica−Amorphous Polymer Nanocomposite Films: The Role of the Polymer Matrix. *ACS Appl. Mater. Interfaces* **2013**, *5*, 5486−5492.

(21) Nelson, J. K.; Fothergill, J. C. Internal Charge Behaviour of Nanocomposites. *Nanotechnology* **2004**, *15*, 586−595.

(22) Tuncer, E.; Sauers, I.; James, D. R.; Ellis, A. R.; Paranthaman, M. P.; Goyal, A.; More, K. L. Enhancement of Dielectric Strength in Nanocomposites. *Nanotechnology* **2007**, *18*, 325704.

(23) McCarthy, D. N.; Stoyanov, H.; Rychkov, D.; Ragusch, H.; Melzer, M.; Kofod, G. Increased Permittivity Nanocomposite Dielectrics by Controlled Interfacial Interactions. *Compos. Sci. Technol.* **2012**, *72*, 731−736.

(24) Ceres, B. V.; Schultz, J. M. Dependence of Electric Breakdown on Spherulite Size in Isotactic Polypropylene. *J. Appl. Polym. Sci.* **1984**, *29*, 4183−4197.

(25) Meth, J. S.; Zane, S. G.; Chi, C. Z.; Londono, J. D.; Wood, B. A.; Cotts, P.; Keating, M.; Guise, W.; Weigand, S. Development of Filler Structure in Colloidal Silica−Polymer Nanocomposites. *Macromolecules* **2011**, *44*, 8301−8313.

(26) Fernandes, N. J.; Koerner, H.; Giannelis, E. P.; Vaia, R. A. Hairy Nanoparticle Assemblies as One-Component Functional Polymer Nanocomposites: Opportunities and Challenges. *MRS Commun.* **2013**, *3*, 13−29.

(27) Hui, C. M.; Dang, A. L.; Chen, B. B.; Yan, J. J.; Konkolewicz, D.; He, H. K.; Ferebee, R.; Bockstaller, M. R.; Matyjaszewski, K. Effect of Thermal Self-Initiation on the Synthesis, Composition, and Properties of Particle Brush Materials. *Macromolecules* **2014**, *47*, 5501−5508.

(28) Pietrasik, J.; Hui, C. M.; Chaladaj, W.; Dong, H.; Choi, J.; Jurczak, J.; Bockstaller, M. R.; Matyjaszewski, K. Silica−Polymethacrylate Hybrid Particles Synthesized Using High-Pressure Atom Transfer Radical Polymerization. *Macromol. Rapid Commun.* **2011**, *32*, 295−311.

(29) Hui, C. M.; Pietrasik, J.; Schmitt, M.; Mahoney, C.; Choi, J.; Bockstaller, M. R.; Matyjaszewski, K. Surface-Initiated Polymerization as an Enabling Tool for Multifunctional (Nano-)Engineered Hybrid Materials. *Chem. Mater.* **2014**, *26*, 745−762.

(30) Matyjaszewski, K.; Tsarevsky, N. V. Macromolecular Engineering by Atom Transfer Radical Polymerization. *J. Am. Chem. Soc.* **2014**, *136*, 6513−6533.

(31) Matyjaszewski, K. Atom Transfer Radical Polymerization (ATRP): Current Status and Future Perspectives. *Macromolecules* **2012**, *45*, 4015−4039.

(32) Ilavsky, J. Nika: Software for Two-Dimensional Data Reduction. *J. Appl. Crystallogr.* **2012**, *45*, 324−328.

(33) Ilavsky, J.; Jemian, P. R. Irena: Tool Suite for Modeling and Analysis of Small-Angle Scattering. *J. Appl. Crystallogr.* **2009**, *42*, 347−353.

(34) Percus, J. K.; Yevick, G. J. Analysis of Classical Statistical Mechanics by Means of Collective Coordinates. *J. Phys. Rev.* **1958**, *110*, 1.

(35) ASTM D149, Standard Test Method for Dielectric Breakdown Voltage and Dielectric Strength of Solid Electrical Insulating Materials at Commercial Power Frequencies. In *1992 Annual Book of ASTM Standards*; American Society for Testing and Materials: Conshohocken, PA, 1992.

(36) Laihonen, S. J.; Gafvert, U.; Schutte, T.; Gedde, U. W. DC Breakdown Strength of Polypropylene Films: Area Dependence and Statistical Behavior. *IEEE Trans. Dielectr. Electr. Insul.* **2007**, *14*, 275−286.

(37) Choi, J.; Hui, C. M.; Pietrasik, J.; Dong, H.; Matyjaszewski, K.; Bockstaller, M. R. Toughening Fragile Matter: Mechanical Properties of Particle Solids Assembled from Polymer-Grafted Hybrid Particles Synthesized by ATRP. *Soft Matter* **2012**, *8*, 4072−4082.

(38) Barbey, R.; Lavanant, L.; Paripovic, D.; Schuwer, N.; Sugnaux, C.; Tugulu, S.; Klok, H. A. Polymer Brushes via Surface-Initiated Controlled Radical Polymerization: Synthesis, Characterization, Properties, and Applications. *Chem. Rev.* **2009**, *109*, 5437−5527.

(39) Kumar, S. K.; Jouault, J. N.; Benicewicz, B.; Neely, T. Nanocomposites with Polymer Grafted Particles. *Macromolecules* **2013**, *46*, 3199−3214.
(40) Tchoul, M. N.; Fillery, S. P.; Koerner, H.; Drummy, L. F.; Oyerokun, F.; Mirau, P. A.; Durstock, M. F.; Vaia, R. A. Assemblies of Titanium Dioxide−Polystyrene Hybrid Nanoparticles for Dielectric Applications. *Chem. Mater.* **2010**, *22*, 1749−1759.
(41) Dinsmore, A. D.; Crocker, J. C.; Yodh, A. G. Self-Assembly of Colloidal Crystals. *Curr. Opin. Colloid Interface Sci.* **1998**, *3*, 5−11.
(42) Nie, Z.; Petukhova, A.; Kumacheva, E. Properties and Emerging Applications of Self-Assembled Structures Made from Inorganic Particles. *Nat. Nanotechnol.* **2009**, *5*, 15−25.
(43) Bruggeman, D. A. G. Berechnung verschiedener physikalischer Konstanten von heterogenen Substanzen. I. Dielektrizitätskonstanten und Leitfähigkeiten der Mischkörper aus isotropen Substanzen. *Ann. Phys. (N.Y.)* **1935**, *24*, 636.
(44) Wu, K.; Dissado, L. A.; Okamoto, T. Percolation Model for Electrical Breakdown in Insulating Polymers. *Appl. Phys. Lett.* **2004**, *85*, 4454−4456.
(45) Roy, M.; Nelson, J. K.; MacCrone, R. K.; Schadler, L. S.; Reed, C. W.; Keefe, R.; Zenger, W. Polymer Nanocomposite Dielectrics - The Role of the Interface. *IEEE Trans. Dielectr. Electr. Insul.* **2005**, *12*, 629−643.
(46) Kobayashi, Y.; Kurosawa, A.; Nagao, D.; Konno, M. Fabrication of Barium Titanate Nanoparticles Polymethylmethacrylate Composite Films and their Dielectric Properties. *Polym. Eng. Sci.* **2009**, *49*, 1069−1075.
(47) Xie, L.; Huang, X.; Wu, C.; Jiang, P. *J. Mater. Chem.* **2011**, *21*, 5897−5906.
(48) Dissado, L. A.; Fothergill, J. C. *Electrical Degradation and Breakdown in Polymers*; P. Peregrinus: London, 1992.
(49) Ma, D.; Siegel, R. W.; Hong, R. I.; Schadler, L. S.; Martensson, E.; Onneby, C. Influence of Nanoparticle Surfaces on the Electrical Breakdown Strength of Nanoparticle-Filled Low-Density Polyethylene. *J. Mater. Res.* **2004**, *19*, 857.
(50) Siddabattuni, S.; Schuman, T. P.; Dogan, F. Dielectric Properties of Polymer−Particle Nanocomposites Influenced by Electronic Nature of Filler Surfaces. *ACS Appl. Mater. Interfaces* **2013**, *5*, 1917−1927.